Journal of Nonlinear Optical Physics & Materials
Vol. 12, No. 2 (2003) 247–261
© World Scientific Publishing Company

World Scientific
www.worldscientific.com

FOURTH-ORDER VARIATIONAL MODE SOLVING FOR ANISOTROPIC PLANAR STRUCTURES

H. P. URANUS* and H. J. W. M. HOEKSTRA

Lightwave Devices Group, MESA+ Research Institute,
University of Twente, P.O. Box 217, 7500 AE Enschede, The Netherlands
**h.p.uranus@el.utwente.nl*

E. VAN GROESEN

Applied Analysis and Mathematical Physics Group, MESA+ Research Institute,
University of Twente, P.O. Box 217, 7500 AE Enschede, The Netherlands

A variational method that gives 4th-order accuracy by only using linear basis functions within the computational domain is proposed for the mode solving of anisotropic planar stratified waveguides with diagonal permitivity tensor. A non-uniform mesh is used to get rid of the necessity of incorporating interface corrections and higher-order basis functions, while Richardson-like extrapolation is used to obtain 4th-order accuracy. The scheme was derived for both TE and TM mode analysis and completed with infinite elements as transparent boundary conditions. The use of a simple extrapolation technique to further refine the results by using two consecutive calculated results is also demonstrated.

Keywords: Variational method; planar waveguide; high accuracy scheme; anisotropic waveguide; transparent boundary conditions.

1. Introduction

Materials that exhibit anisotropy are widely used in realizing integrated optical devices. Among these are ferro-electric crystals like $LiNbO_3$, $LiTaO_3$, KDP, KTP, etc. which have large electro-optic coefficients,[1] amorphous materials like silicon oxynitride (SiO_xN_y) which could be fabricated using silicon-compatible technologies and has relatively wide refractive index range,[2] and poled-polymers with its prospect for realization of cheap devices.[3] Hence, waveguiding analysis of structures with optical anisotropy is important for the design and characterization of such devices.

Accuracy is one of the main issues in numerical and approximate method for optical waveguide analysis. High accuracy is generally preferable, but this feature is usually achieved at the expense of efficiency and introduces more complexity in the method. Variational method with 4th-order accuracy for isotropic structure by using Richardson-like extrapolation has been proposed by Stoffer *et al.*[4] for BPM. In this scheme, linear basis functions are used for regions of uniform index while cubic

basis functions are needed at index discontinuities. Recently, we have proposed a 2nd-order finite difference scheme for anisotropic planar structure with arbitrary index profile.[5] However, due to the necessity to incorporate interface corrections, its extension to higher-order accuracy becomes too complicated for practical applications.

In this paper, we proposed a scheme almost similar to Stoffer's scheme, but instead of using higher-order basis functions at the interfaces, non-uniform meshes are used in order to retain the accuracy and extend the scheme for analyzing anisotropic structure. The scheme does not need complicated interface correction,[6] hence it is simple and requires only modest computational effort. The proposed scheme is completed with infinite elements as the transparent boundary conditions that are exact for homogeneous exterior domains and presented for both TE- and TM-polarized guided-mode analysis of anisotropic planar stratified structures with diagonal permitivity tensor. Although we only present the scheme for 4th-order accuracy, in principle it can be extended to 6th-, 8th-, or even higher-order accuracy with the same simplicity. Additionally, we also introduce a simple extrapolation scheme by using two consecutive calculation results to further refine the results.

This paper is organized as follows. After a brief introduction to the problem, the variational formalism for the problem and its implementation using 1-D finite elements is described. Then, simple upgrade to a higher order scheme by using Richardson-like extrapolation is presented. The application of infinite elements for the transparent boundary conditions and additional extrapolation scheme will then be discussed. The scheme was finally tested by using samples composed of either isotropic or anisotropic materials, which confirms the expected order of accuracy, effectiveness of the boundary conditions and additional extrapolation.

2. Description of the Method

2.1. *Anisotropic planar waveguide*

For anisotropic planar waveguides where the principal axes of the anisotropy are parallel to the Cartesian coordinate system of the waveguide as shown in Fig. 1, the permitivity tensor can be expressed in a diagonal form as

$$\bar{\bar{\varepsilon}} = \varepsilon_0 \begin{bmatrix} n_x^2 & 0 & 0 \\ 0 & n_y^2 & 0 \\ 0 & 0 & n_z^2 \end{bmatrix}. \tag{1}$$

In this paper we assume the z-axis as the propagation direction and that the refractive index varies in the x direction only. As usual, we assume that the waveguide is composed of non-magnetic, source-free, and lossless materials. For this system, it is possible to have uncoupled TE- and TM-polarized waves with corresponding scalar Helmholtz's equations

$$[\partial_{xx} + k_0^2(n_y^2(x) - n_{\text{eff}}^2)]E_y(x) = 0 \quad \text{for TE} \tag{2}$$

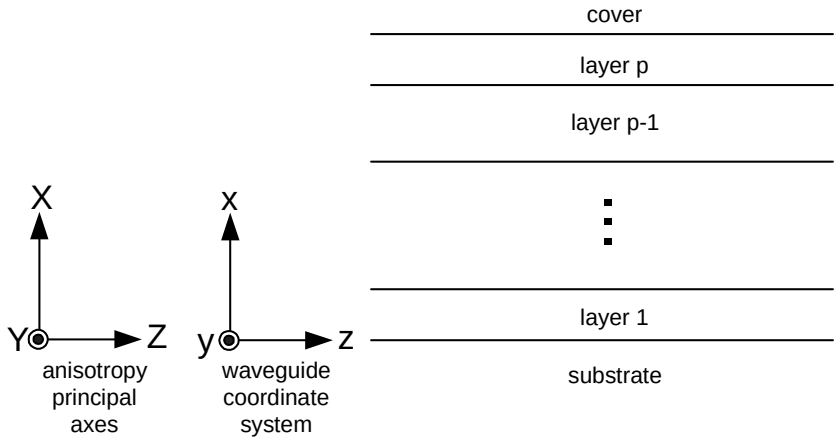

Fig. 1. The structure and its coordinate system.

and

$$\left[\partial_x\left(\frac{1}{n_z^2(x)}\partial_x\right) + k_0^2\left(1 - \frac{n_{\text{eff}}^2}{n_x^2(x)}\right)\right] H_y(x) = 0 \quad \text{for TM}\,. \tag{3}$$

These two scalar Helmholtz's equations will be used throughout this paper. Note that waveguide with isotropic materials (i.e. $n_x^2 = n_y^2 = n_z^2$) is just a special case of this system.

2.2. *Variational method*

The following functionals

$$F_{\text{TE}} = \frac{1}{2}\int_{-\infty}^{\infty} [-(\partial_x E_y(x))^2 + k_0^2(n_y^2(x) - n_{\text{eff}}^2)E_y^2(x)]dx \tag{4}$$

and

$$F_{\text{TM}} = \frac{1}{2}\int_{-\infty}^{\infty} \left[-\frac{1}{n_z^2(x)}(\partial_x H_y(x))^2 + k_0^2\left(1 - \frac{n_{\text{eff}}^2}{n_x^2(x)}\right)H_y^2(x)\right] dx \tag{5}$$

can be derived for partial differential equations (2) and (3), respectively. Since the Euler–Lagrange equations of the functionals correspond to the original modal field equations, the solutions of the latter equations can be approximated by extremization of the functionals. The functions are approximated using the basis functions and the functionals are discretized in finite number of elements within the computational domain, while outside the computational domain, infinite elements (elements that extend to + or − infinity) are used. The extremization of the discretized functionals are then carried out by finding combination of the functions where the gradient of the functional is zero as follows:

$$\nabla\tilde{F} \equiv \left(\frac{\partial\tilde{F}}{\partial\varphi_1}, \frac{\partial\tilde{F}}{\partial\varphi_2}, \ldots, \frac{\partial\tilde{F}}{\partial\varphi_N}\right)^T = (0, 0, \ldots, 0)^T \tag{6}$$

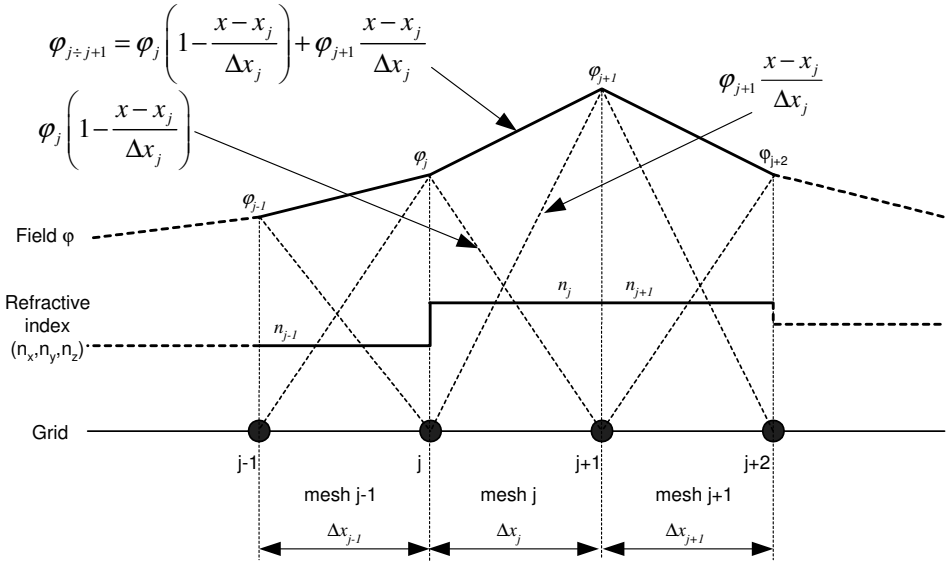

Fig. 2. Linear basis functions and meshes used in the proposed scheme.

with $\tilde{F}$ denoting the discretized functional and N the number of grid points within the computational domain. For convenience, φ_j has been used to denote the value of the function at grid point j, which is $E_{y,j}$ for TE or $H_{y,j}$ for TM wave analysis.

For mesh j, which is not located at the computational boundary and has no interface within it, by expressing the function as expansion of linear basis functions as illustrated in Fig. 2, we will obtain

$$\frac{\partial \tilde{F}}{\partial \varphi_j} = c_{1,j}\varphi_{j-1} + c_{2,j}\varphi_j + c_{3,j}\varphi_{j+1} - n_{\text{eff}}^2(c_{4,j}\varphi_{j-1} + c_{5,j}\varphi_j + c_{6,j}\varphi_{j+1}) \tag{7}$$

for TE-polarized waves, and

$$\frac{\partial \tilde{F}}{\partial \varphi_j} = c_{7,j}\varphi_{j-1} + c_{8,j}\varphi_j + c_{9,j}\varphi_{j+1} - n_{\text{eff}}^2(c_{10,j}\varphi_{j-1} + c_{11,j}\varphi_j + c_{12,j}\varphi_{j+1}) \tag{8}$$

for TM-polarized waves, respectively, with

$$c_{1,j} = \frac{1}{\Delta x_{j-1}} + \frac{1}{6}k_0^2 n_{y,j-1}^2 \Delta x_{j-1} \tag{9a}$$

$$c_{2,j} = -\left(\frac{1}{\Delta x_{j-1}} + \frac{1}{\Delta x_j}\right) + \frac{1}{3}k_0^2(n_{y,j-1}^2 \Delta x_{j-1} + n_{y,j}^2 \Delta x_j) \tag{9b}$$

$$c_{3,j} = \frac{1}{\Delta x_j} + \frac{1}{6}k_0^2 n_{y,j}^2 \Delta x_j \tag{9c}$$

$$c_{4,j} = \frac{1}{6}k_0^2 \Delta x_{j-1} \tag{9d}$$

$$c_{5,j} = \frac{1}{3}k_0^2(\Delta x_{j-1} + \Delta x_j) \tag{9e}$$

$$c_{6,j} = \frac{1}{6}k_0^2\Delta x_j \tag{9f}$$

$$c_{7,j} = \frac{1}{n_{z,j-1}^2\Delta x_{j-1}} + \frac{1}{6}k_0^2\Delta x_{j-1} \tag{9g}$$

$$c_{8,j} = -\left(\frac{1}{n_{z,j-1}^2\Delta x_{j-1}} + \frac{1}{n_{z,j}^2\Delta x_j}\right) + \frac{1}{3}k_0^2(\Delta x_{j-1} + \Delta x_j) \tag{9h}$$

$$c_{9,j} = \frac{1}{n_{z,j}^2\Delta x_j} + \frac{1}{6}k_0^2\Delta x_j \tag{9i}$$

$$c_{10,j} = k_0^2\frac{\Delta x_{j-1}}{6n_{x,j-1}^2} \tag{9j}$$

$$c_{11,j} = \frac{1}{3}k_0^2\left(\frac{\Delta x_{j-1}}{n_{x,j-1}^2} + \frac{\Delta x_j}{n_{x,j}^2}\right) \tag{9k}$$

$$c_{12,j} = k_0^2\frac{\Delta x_j}{6n_{x,j}^2}\,. \tag{9l}$$

Equation (6) can then be written as a generalized matrix eigenvalue equation as

$$\nabla\tilde{F} = (\boldsymbol{A} - n_{\text{eff}}^2\boldsymbol{B})\boldsymbol{\psi} = \boldsymbol{0} \tag{10}$$

with $\boldsymbol{A}$ and $\boldsymbol{B}$ representing tridiagonal matrices with the non-zero elements of their jth row consist of $c_{1,j}\cdots c_{3,j}$ for TE or $c_{7,j}\cdots c_{9,j}$ for TM; and $c_{4,j}\cdots c_{6,j}$ for TE or $c_{10,j}\cdots c_{12,j}$ for TM, respectively. Equation (10) can be solved for its eigenvalues (n_{eff}^2) and its corresponding eigenvectors ($\boldsymbol{\psi}$), which are the approximate solutions of the corresponding Helmholtz's equation.

The use of linear basis functions to approximate the fields in Eqs. (4) and (5) implies that only 3rd-order local error can be obtained for integration at sub-interval located between grid j and $j+1$ as follows:

$$F_{j\div j+1} = \tilde{F}_{j\div j+1}^{\text{lin}} + \Delta x_j^3\ \text{err}(x_{j+\frac{1}{2}}) + O(\Delta x_j^5) \tag{11}$$

which could be evaluated by using Taylor's expansion around $x_{j+\frac{1}{2}}$. In Eq. (11) $F_{j\div j+1}$ denotes the exact value of the functional between grid j and $j+1$, while $\tilde{F}_{j\div j+1}^{\text{lin}}$ the discretized functional using linear basis functions within the same interval. For the case of uniform mesh size, there will be $\Omega/\Delta x$ meshes within the computational domain Ω, which implies only 2nd-order global error of the results.

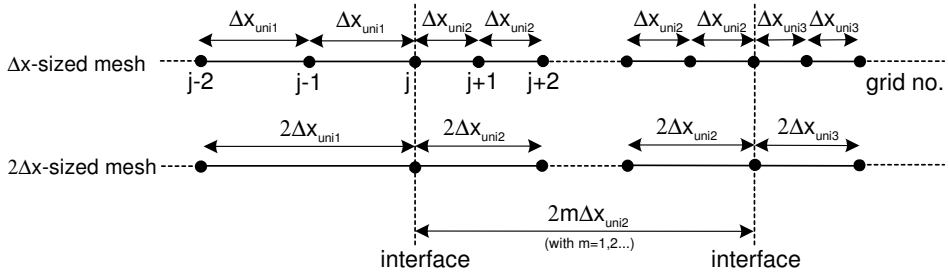

Fig. 3. Mesh-evenization scheme.

2.3. *Richardson-like extrapolation and mesh-evenization scheme*

To achieve 4th-order accuracy, we use Richardson-like extrapolation that combines integration results of different mesh sizes to eliminate the 3rd-order local error term in Eq. (11). By taking $\Delta x_j = \Delta x_{j+1}$ and combine the integration results with the result of $2\Delta x_j$-sized mesh, we could get rid of the 3rd-order error term for local integration interval between grid j and $j+2$ as follows:

$$F_{j\div j+2} = \frac{4}{3}\tilde{F}^{\text{lin}}_{j\div j+2,\Delta x_j} - \frac{1}{3}\tilde{F}^{\text{lin}}_{j\div j+2,2\Delta x_j} + O(\Delta x_j^5) \tag{12}$$

with $\tilde{F}^{\text{lin}}_{j\div j+2,\Delta x_j}$ denotes the integration of the discretized functional between grid j and $j+2$ using linear basis functions for normal-sized (Δx_j-sized) mesh and $\tilde{F}^{\text{lin}}_{j\div j+2,2\Delta x_j}$ for double-sized ($2\Delta x_j$-sized) mesh. In this way, matrices $\boldsymbol{A}$ and $\boldsymbol{B}$ become penta-diagonal.

To keep the scheme simple, we use the slightly non-uniform meshes as depicted in Fig. 3 and hence avoid the necessity of either incorporating complicated interface correction or the use of higher-order basis functions at interfaces to retain the accuracy. To get rid of complicated interface correction we put the grid exactly at the interface, hence the integration within each mesh will not cross the interface. To have the Richardson-like extrapolation to work correctly at interfaces, we have forced the number of normal-sized mesh in-between two adjacent interfaces to be an even number. By this mesh-evenization scheme, none of the integration interval, either the normal- or double-sized interval will cross the interfaces, hence the same form of Eqs. (7)–(9) with proper mesh sizes will remain valid in this formulation and 4th-order-like accuracy can be achieved in a simple way. The scheme can also be extended to 6th-, 8th-, or even higher-order accuracy with the same simplicity.

2.4. *Transparent boundary condition*

A simple transparent boundary condition (TBC) is implemented for guided-wave analysis within this scheme by using 1-D version of infinite element techniques.[7] In this case the mesh outside the computational domain is extended to $-\infty$ at left boundary and to $+\infty$ at the right boundary as shown in Fig. 4, and a proper selection of basis function is made to ensure the convergence of the integration of

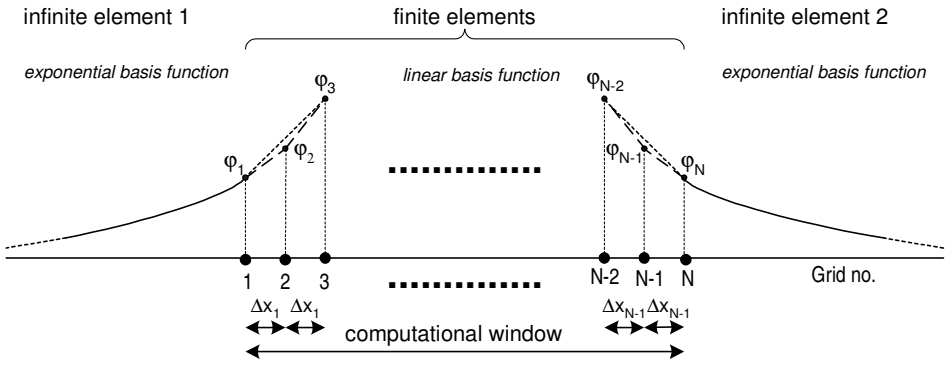

Fig. 4. Infinite elements for transparent boundary conditions for guided mode analysis.

the functional within the element. In this way Eqs. (4) and (5) can be written as

$$F_{\mathrm{TE}} = \frac{1}{2}\int_{-\infty}^{x_1}[-(\partial_x\varphi)^2 + k_0^2(n_{y,s}^2 - n_{\mathrm{eff}}^2)\varphi^2]dx + \sum_{j=1}^{N-1} F_{\mathrm{TE},j}$$

$$+ \frac{1}{2}\int_{x_N}^{+\infty}[-(\partial_x\varphi)^2 + k_0^2(n_{y,c}^2 - n_{\mathrm{eff}}^2)\varphi^2]dx \tag{13}$$

and

$$F_{\mathrm{TM}} = \frac{1}{2}\int_{-\infty}^{x_1}\left[-\frac{1}{n_{z,s}^2}(\partial_x\varphi)^2 + k_0^2\left(1 - \frac{n_{\mathrm{eff}}^2}{n_{x,s}^2}\right)\varphi^2\right]dx + \sum_{j=1}^{N-1} F_{\mathrm{TM},j}$$

$$+ \frac{1}{2}\int_{x_N}^{+\infty}\left[-\frac{1}{n_{z,c}^2}(\partial_x\varphi)^2 + k_0^2\left(1 - \frac{n_{\mathrm{eff}}^2}{n_{x,c}^2}\right)\varphi^2\right]dx \tag{14}$$

for TE- and TM-polarized wave, respectively. In these equations, subscripts s and c denote the substrate and cover of the structure, respectively. It is assumed that the substrate is located at the left and the cover at the right hand side of the structure. For guided mode analysis, we can use exponential basis function as denoted in Fig. 4 for the infinite element. For TE mode analysis, we use

$$\varphi(x) = \varphi_1 \exp[k_0\sqrt{n_{\mathrm{eff}}^2 - n_{y,s}^2}(x - x_1)] \tag{15a}$$

and

$$\varphi(x) = \varphi_N \exp[-k_0\sqrt{n_{\mathrm{eff}}^2 - n_{y,c}^2}(x - x_N)] \tag{15b}$$

while for TM mode analysis we use

$$\varphi(x) = \varphi_1 \exp\left[k_0\frac{n_{z,s}}{n_{x,s}}\sqrt{n_{\mathrm{eff}}^2 - n_{x,s}^2}(x - x_1)\right] \tag{16a}$$

and

$$\varphi(x) = \varphi_N \exp\left[-k_0\frac{n_{z,c}}{n_{x,c}}\sqrt{n_{\mathrm{eff}}^2 - n_{x,c}^2}(x - x_N)\right] \tag{16b}$$

for infinite element 1 and 2, respectively. Since these functions are the exact solutions of guided waves for homogeneous exterior domains, the use of these exponential basis functions will give exact transparent boundary conditions. As a result, the functionals can be written as

$$F_{\mathrm{TE}} = -\frac{1}{2}k_0\sqrt{n_{\mathrm{eff}}^2 - n_{y,s}^2}\varphi_1^2 + \sum_{j=1}^{N-1} F_{\mathrm{TE},j} - \frac{1}{2}k_0\sqrt{n_{\mathrm{eff}}^2 - n_{y,c}^2}\varphi_N^2 \tag{17}$$

and

$$F_{\mathrm{TM}} = -\frac{1}{2}k_0\frac{\sqrt{n_{\mathrm{eff}}^2 - n_{x,s}^2}}{n_{x,s}n_{z,s}}\varphi_1^2 + \sum_{j=1}^{N-1} F_{\mathrm{TM},j} - \frac{1}{2}k_0\frac{\sqrt{n_{\mathrm{eff}}^2 - n_{x,c}^2}}{n_{x,c}n_{z,c}}\varphi_N^2 \tag{18}$$

for the TE and TM polarized wave, respectively. This implies that the $\frac{\partial \tilde{F}}{\partial \varphi_1}$ and $\frac{\partial \tilde{F}}{\partial \varphi_N}$ (first and last rows in matrix $\boldsymbol{A}$ and $\boldsymbol{B}$) differ from the other rows as follows:

$$\frac{\partial \tilde{F}}{\partial \varphi_1} = c_{2,1}\varphi_1 + c_{3,1}\varphi_2 - n_{\mathrm{eff}}^2(c_{5,1}\varphi_1 + c_{6,1}\varphi_2) \tag{19}$$

$$\frac{\partial \tilde{F}}{\partial \varphi_N} = c_{1,N}\varphi_{N-1} + c_{2,N}\varphi_N - n_{\mathrm{eff}}^2(c_{4,N}\varphi_{N-1} + c_{5,N}\varphi_N) \tag{20}$$

for TE, and

$$\frac{\partial \tilde{F}}{\partial \varphi_1} = c_{8,1}\varphi_1 + c_{9,1}\varphi_2 - n_{\mathrm{eff}}^2(c_{11,1}\varphi_1 + c_{12,1}\varphi_2) \tag{21}$$

$$\frac{\partial \tilde{F}}{\partial \varphi_N} = c_{7,N}\varphi_{N-1} + c_{8,N}\varphi_N - n_{\mathrm{eff}}^2(c_{10,N}\varphi_{N-1} + c_{11,N}\varphi_N) \tag{22}$$

for TM, respectively, with

$$c_{2,1} = -\frac{1}{\Delta x_1} + \frac{1}{3}k_0^2 n_{y,1}^2 \Delta x_1 - k_0\sqrt{n_{\mathrm{eff}}^2 - n_{y,s}^2} \tag{23a}$$

$$c_{2,N} = -\frac{1}{\Delta x_{N-1}} + \frac{1}{3}k_0^2 n_{y,N-1}^2 \Delta x_{N-1} - k_0\sqrt{n_{\mathrm{eff}}^2 - n_{y,c}^2} \tag{23b}$$

$$c_{5,1} = \frac{1}{3}k_0^2 \Delta x_1 \tag{23c}$$

$$c_{5,N} = \frac{1}{3}k_0^2 \Delta x_{N-1} \tag{23d}$$

$$c_{8,1} = -\frac{1}{n_{z,1}^2 \Delta x_1} + \frac{1}{3}k_0^2 \Delta x_1 - k_0\frac{\sqrt{n_{\mathrm{eff}}^2 - n_{x,s}^2}}{n_{x,s}n_{z,s}} \tag{23e}$$

$$c_{8,N} = -\frac{1}{n_{z,N-1}^2 \Delta x_{N-1}} + \frac{1}{3}k_0^2 \Delta x_{N-1} - k_0\frac{\sqrt{n_{\mathrm{eff}}^2 - n_{x,c}^2}}{n_{x,c}n_{z,c}} \tag{23f}$$

$$c_{11,1} = \frac{1}{3}k_0^2 \frac{\Delta x_1}{n_{x,1}^2} \tag{23g}$$

$$c_{11,N} = \frac{1}{3}k_0^2 \frac{\Delta x_{N-1}}{n_{x,N-1}^2} \tag{23h}$$

while $c_{3,1}$, $c_{6,1}$, $c_{1,N}$, $c_{4,N}$, $c_{9,1}$, $c_{12,1}$, $c_{7,N}$, and $c_{10,N}$ remain the same as in Eq. (9). The last terms of Eqs. (23a), (23b), (23e), and (23f) are contributed by the infinite elements.

The boundary conditions induce non-linearity to the generalized eigenvalue equation. The solutions of this eigenvalue equation can then be obtained by using iterative algorithm by using results obtained by Dirichlet boundary condition (DBC) as initial values for n_{eff} terms in Eq. (23). Since every mode needs its own optimized value of n_{eff}, the iteration will become a two-loop iteration scheme. Alternatively, we can also use root searching algorithm to solve the dispersion relation $\det(\boldsymbol{A} - n_{\text{eff}}^2 \boldsymbol{B}) = \boldsymbol{0}$ which is the one employed throughout this paper.

2.5. *Additional extrapolation*

As will be shown later, by proper choice of average mesh size and neglecting higher order terms, the error profile of the results of the proposed scheme will be given by

$$\text{ord} \simeq \frac{\log(\text{Err}_k/\text{Err}_l)}{\log(\Delta\bar{x}_k/\Delta\bar{x}_l)} \tag{24}$$

with ord denotes the order of accuracy (2 for scheme without and 4 for scheme with Richardson-like extrapolation), $\Delta\bar{x}_k$ and $\Delta\bar{x}_l$ the average mesh sizes for kth and lth computation, respectively, while Err_k and Err_l are relative errors in the calculated effective indices of corresponding computations which can be expressed as

$$\text{Err}_\eta = \frac{|n_{\text{eff,calc\_}\eta} - n_{\text{eff,ex}}|}{n_{\text{eff,ex}}} \quad \text{with } \eta = k, l\,. \tag{25}$$

In Eq. (25) and $n_{\text{eff,calc\_}k}$ and $n_{\text{eff,calc\_}l}$ denote effective indices resulted from kth and lth computation, respectively, while $n_{\text{eff,ex}}$ denotes the exact effective index. This relation can be used to further refine the results by using calculated results taken from two different mesh sizes. By substituting Eq. (25) into Eq. (24), we arrive at

$$n_{\text{eff,extrapolate}} = \frac{\left(\frac{\Delta\bar{x}_k}{\Delta\bar{x}_l}\right)^{\text{ord}} n_{\text{eff,calc\_}l} - n_{\text{eff,calc\_}k}}{\left(\frac{\Delta\bar{x}_k}{\Delta\bar{x}_l}\right)^{\text{ord}} - 1}\,. \tag{26}$$

In Eq. (26) we have taken $\text{sign}(n_{\text{eff,calc\_}k} - n_{\text{eff,ex}}) = \text{sign}(n_{\text{eff,calc\_}l} - n_{\text{eff,ex}})$, which comes from the systematic property of the error term in Eqs. (11) and (12).

Since a small fluctuation remains in the computational results induced by the slightly non-uniform discretization scheme, better results could be achieved by using more calculated points and implementing data fitting techniques.

3. Numerical Results

3.1. *Isotropic waveguide*

The first sample is a 3-layer isotropic structure with sub-wavelength film thickness and high index contrast corresponding to an air-GaAs-air structure[8] with refractive indices at $\lambda = 0.86$ μm for the substrate, film, and cover layers given by $n_s = 1$, $n_f = 3.6$, and $n_c = 1$, respectively, while the film thickness given as 0.6 μm. The results for fundamental and highest order TM-polarized modes that are carried out by using a computational window that has exactly the same size as the width of the guiding layer (only 0.6 μm) is shown in Fig. 5 for relative error in n_{eff} as defined by Eq. (25). The exact values of effective index of this structure are calculated using transfer matrix method (TMM). Even with such a small computational window, the implemented TBC already gives nice results, while the DBC suffers from the error caused by the incorrect representation of the field at the computational boundary even when a larger computational window (0.7 μm) is used. This superiority is more pronounced in the 4th- (highest-) order mode analysis. In this case, the DBC does not give any results unless the computational window is enlarged to 0.9 μm, while the TBC gives good results starting from 0.6 μm. Almost the same error profile was also obtained for TE polarization analysis. These results confirm the expected order of accuracy of the proposed scheme, which are 2nd-order for scheme without and 4th-order for scheme with Richardson-like extrapolation.

3.2. *Anisotropic waveguide*

For anisotropic waveguide sample, we choose a 4-layer waveguide with isotropic substrate and cover and with 2 birefringent films.[9] The sample is composed of SiO_2 substrate with silicon oxynitride (SiO_xN_y) and calix[4]arene films on top of it and air as the covering layer. For light with wavelength of 957.44 nm, the refractive indices of SiO_2, SiO_xN_y, calix[4]arene, and air are $n_x = n_y = n_z = 1.4526$, $n_x = 1.6721$ $n_y = n_z = 1.6738$, $n_x = 1.5630$ $n_y = n_z = 1.5622$, and $n_x = n_y = n_z = 1$, respectively. The thickness of the SiO_xN_y and calix[4]arene are 591 nm and 600 nm, respectively. There are 2 guided-modes for this structure, and the results for TE_0 and TM_0 modes are shown in Fig. 6. Again, the exact values of effective indices of this structure are calculated using TMM[10] formulated for anisotropic media, and the calculation for the scheme with TBC was carried out using computational window of the size exactly the same as the thickness of the guiding region. As shown in the figure, the order of the accuracy is as expected and the results of the scheme with TBC are much better than the one with DBC.

3.3. *Effect of computational window size*

To further demonstrate the contribution of the transparent boundary condition, we calculate the isotropic structure discussed earlier by using different window sizes. The results are depicted in Fig. 7. As visible from the results, the application

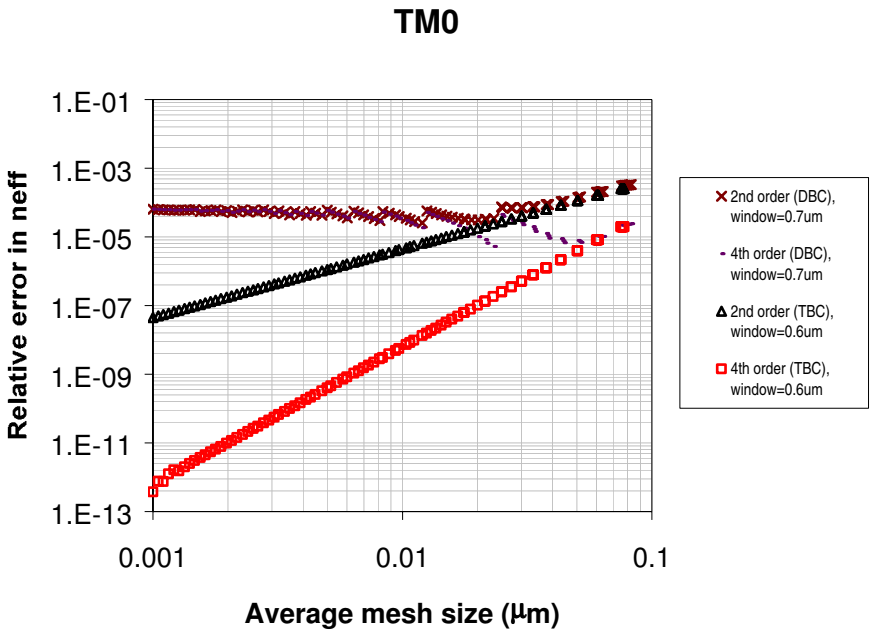

(a)

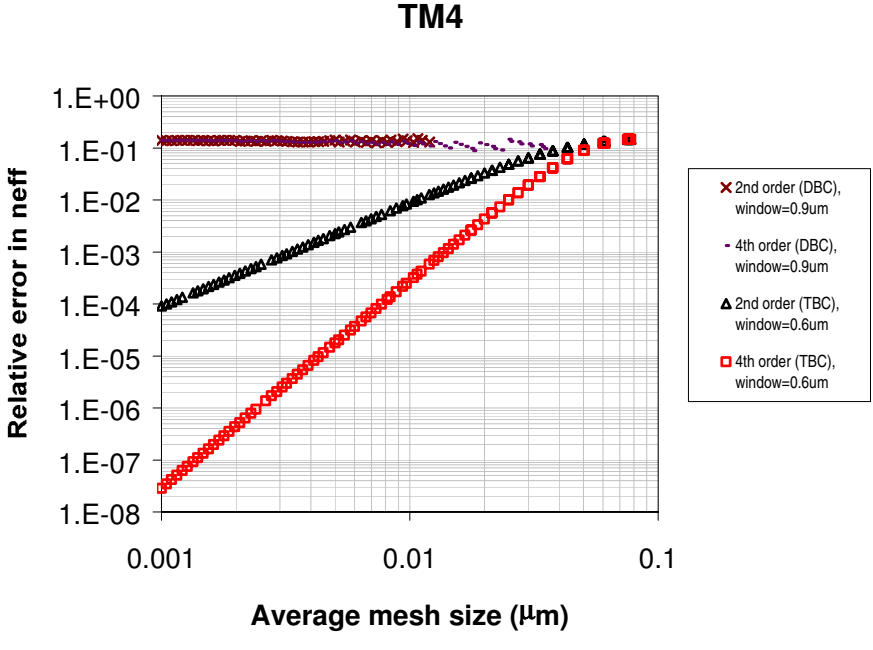

(b)

Fig. 5. Results of 3-layer high-contrast isotropic waveguide (a) TM_0 mode (b) TM_4 mode.

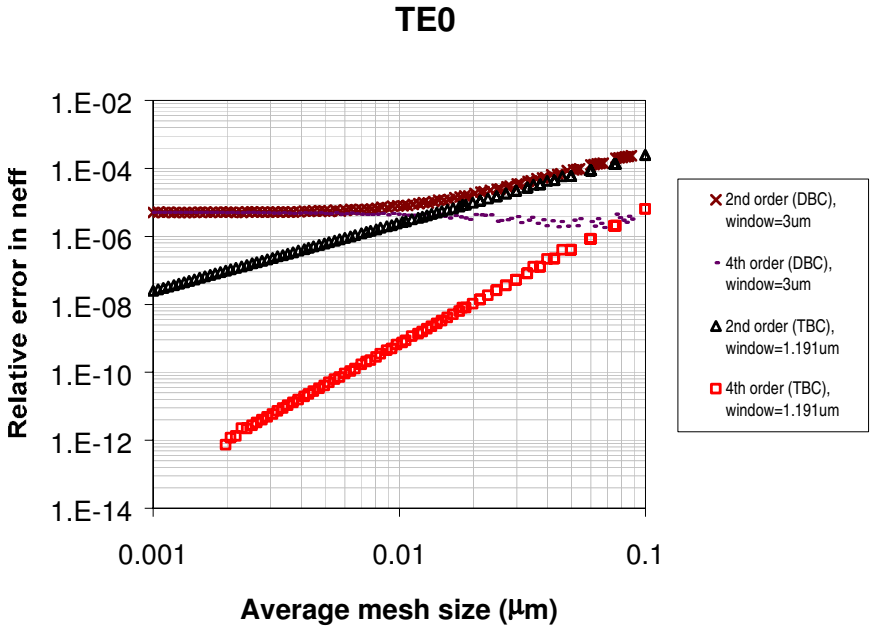

(a)

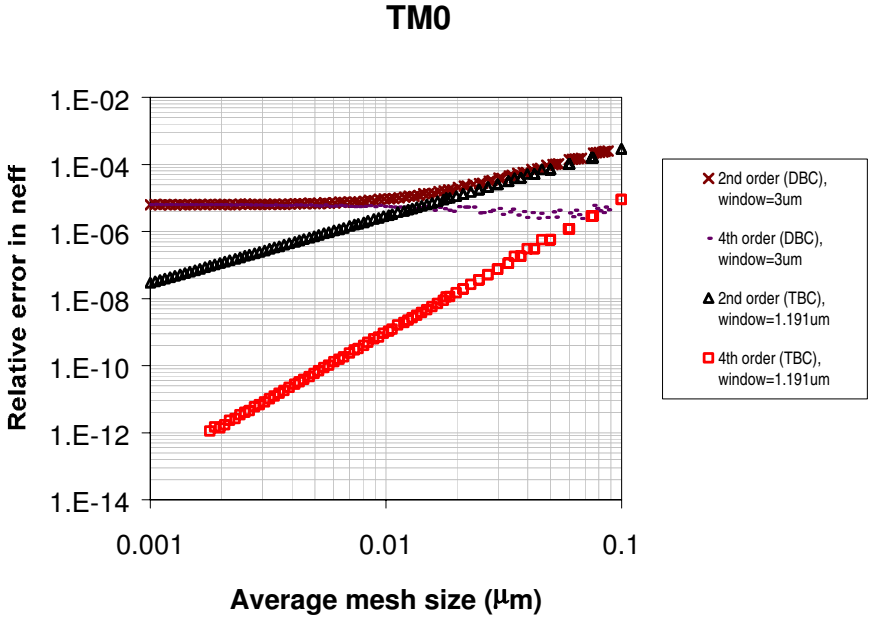

(b)

Fig. 6. The results for 4-layer asymmetric waveguide with birefringent films (a) TE_0 (b) TM_0.

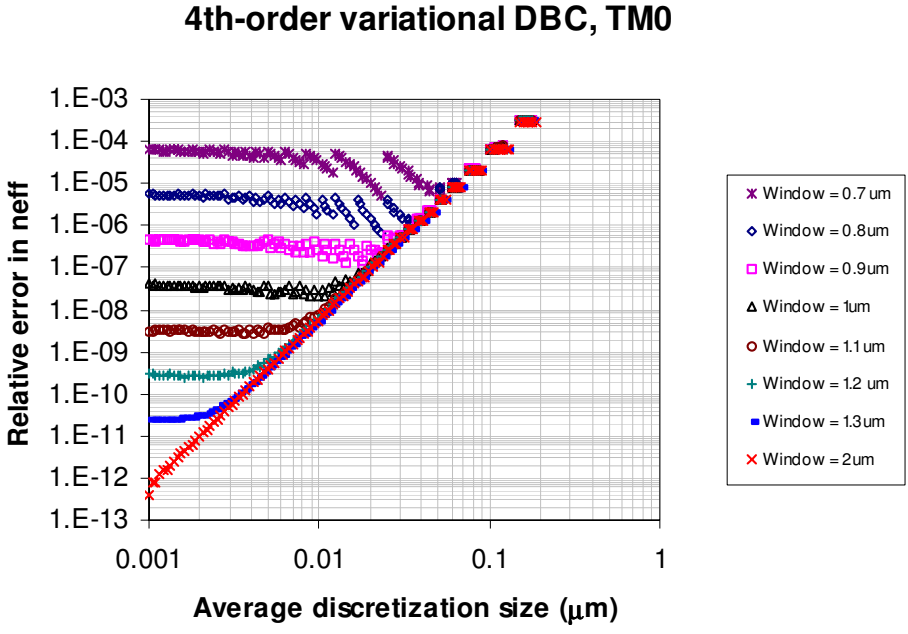

(a)

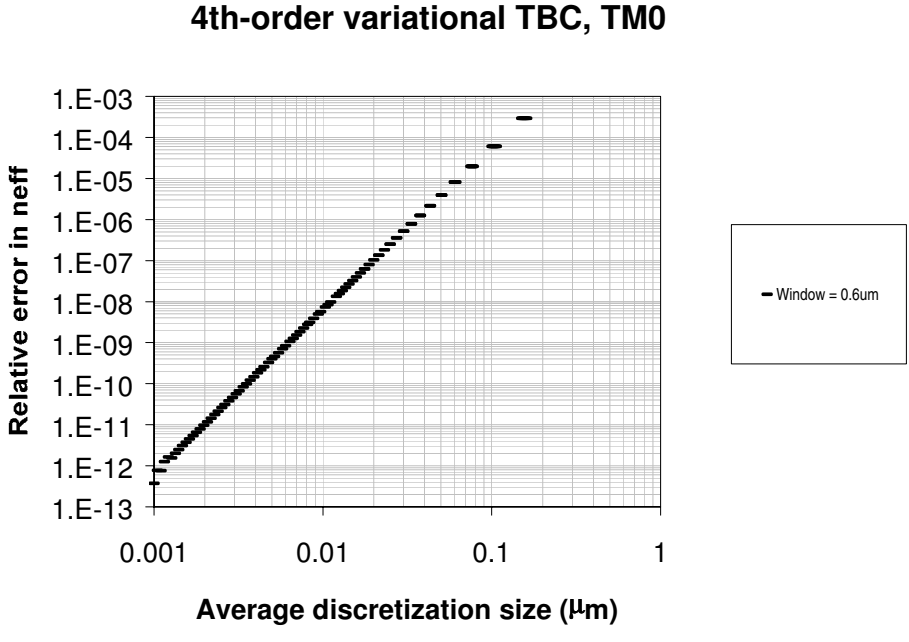

(b)

Fig. 7. The effect of window size for TM_0 analysis of the 3-layer isotropic waveguide (a) 4th-order scheme with DBC (b) 4th-order scheme with TBC.

Table 1. Extrapolation using 2nd-order results of 4-layer anisotropic sample.

	Before extrapolation				After extrapolation
Mode	$\Delta\bar{x}_k$ (nm)	Err_k	$\Delta\bar{x}_l$ (nm)	Err_l	Err
TE0	100	$2.45E-4$	30	$2.20E-5$	$3.83E-7$
TE1	100	$9.46E-4$	30	$8.61E-5$	$2.72E-6$
TM0	30	$2.57E-5$	3	$2.72E-7$	$3.33E-9$
TM1	30	$9.24E-5$	3	$9.78E-7$	$9.74E-9$

Table 2. Extrapolation using 4th-order results of 4-layer anisotropic sample.

	Before extrapolation				After extrapolation
Mode	$\Delta\bar{x}_k$ (nm)	Err_k	$\Delta\bar{x}_l$ (nm)	Err_l	Err
TE0	100	$6.39E-6$	30	$5.26E-8$	$2.81E-9$
TE1	100	$1.01E-4$	30	$8.61E-7$	$7.30E-8$
TM0	30	$7.40E-8$	3	$8.28E-12$	$1.43E-13$
TM1	30	$9.58E-7$	3	$1.08E-10$	$2.88E-12$

of TBC minimizes the error caused by incorrect field values at the boundaries, which allows the computation to be carried out in a relatively small computational window, even as small as the thickness of the guiding region.

3.4. *Extrapolation results*

As could be seen from the results of the scheme with transparent boundary conditions, for proper discretization size, the error profile follows Eq. (24), hence we could use results from two consecutive calculations with different mesh sizes to further refine the results. Tables 1 and 2 show the extrapolated results for the 4-layer anisotropic structure discussed earlier by using 2nd- and 4th-order calculation results, respectively. The results are presented in terms of relative error in effective indices, which have been truncated to a few digits for clarity. All these results are obtained by computational window size of 1.191 μm, which is just the thickness of the guiding region. These tables clearly show the refinement of the computational results by means of the simple extrapolation scheme.

4. Conclusions

A simple variational scheme for modal analysis of anisotropic step-index planar waveguides with diagonal permitivity tensor is proposed. The scheme uses non-uniform mesh and Richardson-like extrapolation to achieve 4th-order accuracy without any interface correction, using only simple linear basis function within the computational domain. The scheme is furnished with infinite elements as the transparent boundary conditions that allow the computation to be carried out in the smallest possible computational window. Further refinement of the results by extrapolating two consecutive computational results were also demonstrated.

Acknowledgment

This work is supported by STW Technology Foundation through project TWI.4813.

References

1. E. L. Wooten, K. M. Kissa, A. Y. Yan, E. J. Murphy, D. A. Lafaw, P. F. Hallemeier, D. Maack, D. V. Attanasio, D. J. Fritz, G. J. McBrein and D. E. Bossi, *J. Sel. Top. Quantum Electron.* **6**, 69 (2000).
2. K. Wörhoff, P. V. Lambeck and A. Driessen, *J. Lightwave Tech.* **17**, 1401 (1999).
3. M. C. Oh, H. Zhang, C. Zhang, H. Erlig, Y. Chiang, B. Tsap, D. Chang, A. Szep, W. H. Steier, H. R. Fetterman and L. R. Dalton, *J. Sel. Top. Quantum Electron.* **7**, 826 (2001).
4. R. Stoffer, P. A. A. J. Bollerman, H. J. W. M. Hoekstra, E. van Groesen and F. P. H. van Beckum, *Opt. Quantum Electron.* **31**, 705 (1999).
5. H. P. Uranus, H. J. W. M. Hoekstra and E. van Groesen, *Opt. Quantum Electron.* **35**, 407 (2003).
6. H. P. Uranus, H. J. W. M. Hoekstra and E. van Groesen, "Fourth-order accurate variational planar mode solver," internal technical report, LDG & AAMP, Univ. Twente, 2001.
7. M. J. McDougall and J. P. Webb, *IEEE Trans. Microwave Theory Tech.* **37**, 1724 (1989).
8. H. A. Jamid and M. N. Akram, *J. Lightwave Tech.* **19**, 398 (2001).
9. H. J. W. M. Hoekstra, O. Noordman, G. J. M. Krijnen, R. K. Varshney and E. Henselmans, *J. Opt. Soc. Am.* **B14**, 1823 (1997).
10. C. K. Chen, P. Berini, D. Z. Feng, S. Tanev and V. P. Tzolov, *Opt. Exp.* **7**, 260 (2000).